Early-Age Cracking in Reconstructed Concrete Bridge Barrier Walls

Daniel CUSSON and Wellington L. REPETTE

Institute for Research in Construction
National Research Council Canada
Ottawa, Ontario, Canada K1A 0R6

Originally published in ACI Materials Journal, 97(4), July-August 2000, pp. 438-446.

Abstract: An assessment of newly reconstructed reinforced concrete barrier walls on a highway bridge near Montreal indicated intense transverse cracking only a few days after concreting. Subsequent inspection of other concrete bridges in urban areas confirmed that such cracking is not uncommon. Analytical models, together with field and estimated data, were used to study the magnitude and roles of the factors that are the probable cause of this cracking. The results indicate that a combination of factors, such as temperature gradients, differential shrinkage and vibration due to traffic circulation, generated stresses that exceeded the low tensile strength of the young concrete.

Résumé: Une inspection des parapets en béton armé nouvellement reconstruits d'un pont d'autoroute près de Montréal a révélé une fissuration transversale intense seulement quelques jours après le bétonnage. Une inspection subséquente d'autres ponts en béton situés dans des régions urbaines a confirmé qu'une telle fissuration n'était pas inhabituelle. Des modèles analytiques, supportés par des données in-situ et estimées, ont été utilisés afin d'étudier l'importance et le rôle des facteurs qui sont la cause probable de cette fissuration. Les résultats indiquent qu'une combinaison de facteurs, tels les gradients de température, le retrait différentiel et la vibration due à la circulation, a produit des contraintes qui ont excédées la faible résistance en tension du jeune béton.

RESEARCH SIGNIFICANCE

Major factors that contributed to the early-age cracking of a reconstructed concrete bridge barrier wall were evaluated using analytical models from the CEB (1993a) and ACI 209 (1997) design codes along with measured field data and finite element modeling. A sound understanding of the early-age cracking problem is important because it may lead to ingress of moisture and salt, reinforcement corrosion, concrete spalling and, ultimately, to a reduced in-service performance of the bridge. The conclusions obtained from this study can also be applied to newly constructed barrier walls since they are often built several weeks or months after the bridge slab.

INTRODUCTION

A survey to 52 departments of transportation across North America revealed that more than 100,000 bridges in the U.S. – about half of the bridges monitored by the respondents – had developed transverse cracking of the deck after construction (TRB 1996). It is known that such cracking eventually leads to corrosion of the reinforcing steel and spalling of the protective concrete cover, resulting in increased maintenance costs and reduced service life of the affected structure.

This paper presents an analytical assessment of the possible causes of early-age cracking observed in reconstructed reinforced concrete barrier walls on the recently rehabilitated Vachon Bridge near Montreal, Canada.

Rehabilitation of Vachon Bridge

In 1996, *Ministère des transports du Québec* (MTQ) undertook a major rehabilitation of the Vachon Bridge, located north of Montreal at the intersection of Highway 13 and the Mille-Îles river. The work involved patching the concrete slab and replacing the barrier walls, the waterproofing membrane, and the asphalt-wearing course. The bridge, 714 m in length, has 21 simply supported spans of reinforced concrete slab on prestressed concrete girders.

A group of ten spans of a barrier wall, each 34 m long, had previously been selected for tests on corrosion inhibiting systems installed during the rehabilitation. A detailed description of the study on the in-situ performance of various corrosion inhibiting systems can be found in Cusson and Mailvaganam (1999).

The placing of concrete in the barrier wall occurred in mid-October 1996. As given in Table 1, the concrete contained 450 kg/m^3 of Type 10 cement (ASTM Type 1) and had a water-cement ratio (*w/c*) of 0.36.

Table 1 – Mix design of barrier wall concrete

Constituents	Quantity per m^3
Crushed stone, 20 mm	361 kg
Crushed stone, 14 mm	361 kg
Crushed stone, 10 mm	309 kg
Sand	702 kg
Cement, Type 10	450 kg
Water	160 kg
Water reducer	1125 ml
Air entrainer	315 ml
Superplasticizer	1500 ml
w/c	0.36

The fresh concrete had a slump of 80 mm and an air content of 6.5%. The steel reinforcement consisted of eight 15 mm longitudinal bars in the cross-section and 15 mm transverse bars spaced at 230 mm along the barrier wall length. The formwork was made of steel panels on the traffic-exposed face of the barrier wall and plywood panels at the back. The upper surface of the barrier wall was covered with wet burlap until the formwork was removed approximately 24 h after concreting. The concrete had an average 28-day compressive strength of 45 MPa, determined from 150 x 300 mm cylinders cured in a moist room until testing.

Observation of transverse cracking after rehabilitation

An inspection of the barrier walls, carried out 1-1/2 days after casting (12 h after form removal), revealed closely spaced cracks running completely through the walls; this raised a concern for premature reinforcing bar corrosion due to moisture and salt ingress. The cracks had an average spacing of 0.80 m (comparable to the 0.9 m height of the barrier wall), and were mostly located at midspan. No joints other than the expansion joints between each 34 m long span were present to control crack spacing. Most cracks had a width of 0.2 mm or less, with a few having openings of 0.3 mm.

Figure 1 presents a picture taken 7 months after rehabilitation, illustrating the transverse cracking in the barrier wall. At that time, new cracks had occurred, resulting in an average crack spacing of 0.75 m with a uniform distribution of cracks along the entire span of the barrier wall.

ANALYSIS OF FACTORS GOVERNING CRACKING

The main factors likely to govern early-age cracking are presented in this section. In the following section, they are incorporated into a global structural model for the computation of the total stress causing cracking. The following assumptions were made: a) concrete behaves as a linear elastic material in tension; b) the barrier wall was fully restrained at the base by the deck slab; c) equations for the estimation of concrete properties, shrinkage, and relaxation defined in the CEB (1933a) and ACI-209 (1997) design codes are valid for concretes as young as 12 h of age; and d) the superposition principle is valid for all time increments.

Measured data of the field conditions were used as input for the analytical models employed for the calculation of the main concrete properties and various types of strains and stresses affecting cracking. For instance, recorded variations of ambient temperature and ambient relative humidity, shown in Fig. 2, were used in the determination of time-dependent concrete conditions and properties such as temperature profiles, concrete maturity, tensile strength, modulus of elasticity, shrinkage, and creep. Strain gages embedded in the concrete of the barrier walls were used to measure vibration-induced strains due to traffic that was allowed on the bridge during rehabilitation.

Fig. 1 – Transverse cracking observed in concrete barrier walls after rehabilitation

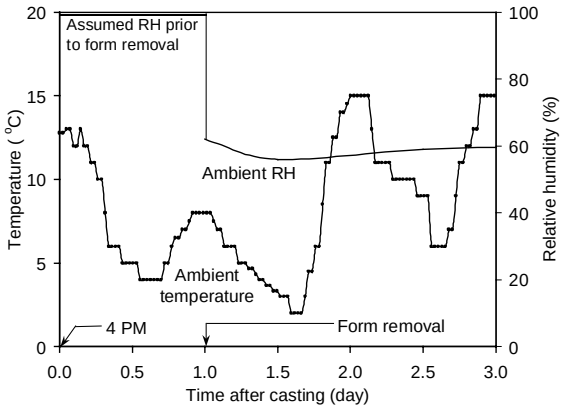

Fig. 2 – Measured ambient temperature and ambient relative humidity

The most important equations from the CEB (1993a) and ACI 209 (1997) design codes that were used in this study are presented in this section, and supplementary equations and parameters in Appendixes 1 and 2, respectively.

Concrete tensile strength and modulus of elasticity

The low tensile strength of concrete makes it susceptible to cracking, particularly during the first days after placing. The time-dependent development of the tensile strength (Fig. 3) and modulus of elasticity (Fig. 4) of the concrete were calculated for the conditions measured in the field using the equations proposed in CEB (1993a).

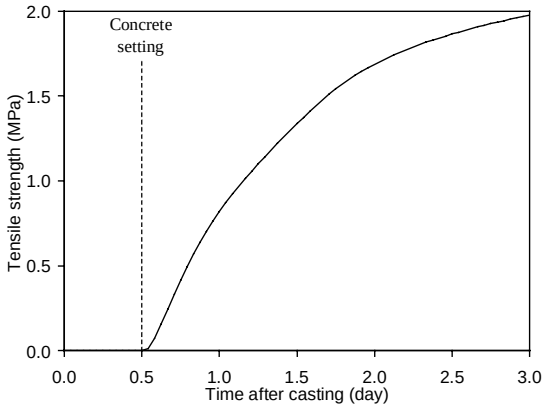

Fig. 3 – Estimated tensile strength of barrier wall concrete

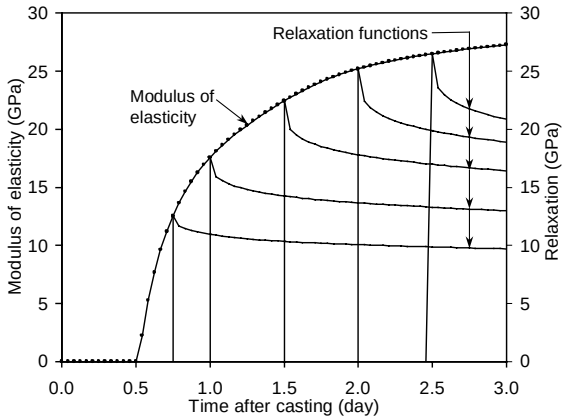

Fig. 4 – Estimated modulus of elasticity and relaxation functions of barrier wall concrete

A setting time of 12 h was estimated based on field observation. Since the concrete of the barrier wall was cured at temperatures lower than 20°C, the determination of the concrete maturity was necessary to account for the slower development of the tensile strength and modulus of elasticity. Maturity was calculated using the estimated average concrete temperature in the barrier wall as a function of time, which, in turn was based on the measured ambient temperature.

Restraints

External restraint – In a new barrier wall cast over an old deck slab, significant external restraint can be generated by the slab whose concrete is more mature and stable (superior stiffness, negligible shrinkage and creep, and smaller thermal expansion coefficient) than the young concrete of the barrier wall. Significant stresses can therefore result. According to ACI 207 (1995), unreinforced walls, fully restrained at their base can ultimately attain full-section cracks spaced at one to two times the height of the wall. The observed spacing of the cracks in the barrier wall, approximately 0.8 times the height of the wall, agrees well with this, suggesting that near full restraint was imposed by the deck slab. The crack spacing was smaller than the wall height due to the presence of steel reinforcement (ρ_g = 0.4%) that generated some additional restraint at crack locations.

The restrained strain ε_R within the barrier wall concrete was calculated as follows:

[1] $$\varepsilon_R = K_R \cdot \varepsilon_f$$

where K_R is the degree of restraint varying from 0 (movement unrestrained) to 1 (movement fully restrained), and ε_f is the free strain. The degree of external restraint in a barrier wall depends mainly on the vertical distance d measured from the slab/wall interface (K_R = 1 at the interface) and its length-height ratio L/H (K_R = 1 regardless of d when L/H tends toward infinity).

The degree of external restraint was obtained by using the following equation, which has been developed for unreinforced concrete walls (ACI Committee 207 1995):

[2] $$K_R = \left(\frac{L/H - 1}{L/H + 10}\right)^{d/H} \quad \text{for L/H<2.5}$$

or

$$K_R = \left(\frac{L/H - 2}{L/H + 1}\right)^{d/H} \quad \text{for L/H}\geq 2.5$$

Equation [2] may underestimate the degree of external restraint for steel-reinforced concrete walls. A three-dimensional elastic finite element (FE) analysis performed by the authors (Fig. 5), indicated that this underestimation is not significant (< 15%) for a wall with L/H = 1 and a reinforcement ratio ρ_g = 0.4%. This underestimation becomes less significant with decreasing d and increasing L/H. The L/H of 1 was selected in the FE analysis because it corresponded well to field observations of cracking, with L taken as the length between two adjacent cracks. The figure also illustrates good agreement between the numerical analysis and a laboratory experiment conducted by Carlson and Reading (1988) for an unreinforced wall with L/H = 1.

Another set of results from the FE analysis presented in Fig. 6 indicated that, for a given height, the degree of external restraint remained relatively constant across the wall thickness. This observation confirms the validity of not taking the barrier wall thickness into account in Eq. [2]. Small negative K_r values were found at the top of the unreinforced wall (L/H = 1), indicating the occurrence of small compressive stresses.

To account for the stiffness difference between the newly cast barrier wall and the more mature deck slab, the nominal degree of external restraint calculated with Eq. [2] was multiplied by the stiffness ratio defined in Eq. [3]:

$$[3] \qquad R_s = \frac{A_s E_s}{A_s E_s + A_w E_w}$$

where A_s and A_w are the cross-sectional areas of the deck slab and the barrier wall, respectively, and E_s and E_w are the moduli of elasticity of the concrete in the deck slab and the barrier wall, respectively.

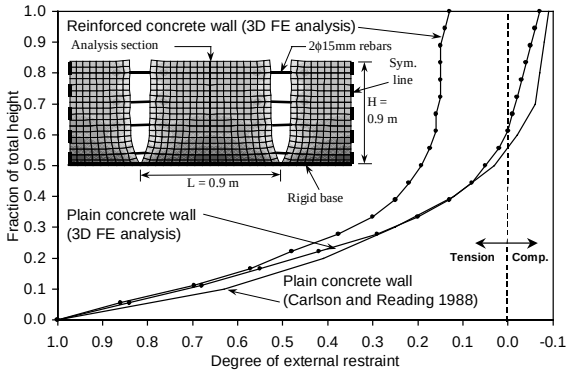

Fig. 5 – Estimated external restraint in plain and reinforced concrete walls with L/H=1 (elevation view of the wall model)

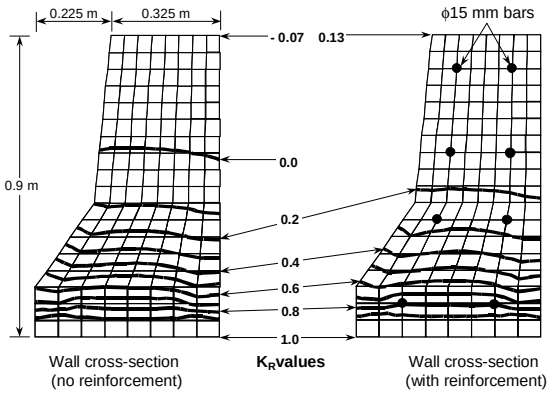

Fig. 6 – Estimated external restraint in plain and reinforced concrete walls with L/H=1 (cross section view of the wall model)

The value of A_s effective in restraining the barrier wall was assumed to be 2.5 A_w, in line with similar assumption for concrete walls cast on rock foundations (ACI Committee 207 1995). The stiffness ratio equaled 1.0 before concrete setting (E_w/E_s = 0), and decreased with the increase of E_w to a value of 0.76 three days after casting (E_w/E_s = 0.78).

Internal restraint – Internal restraint is generated as a result of nonuniform distribution of movement across the wall thickness due to factors such as temperature and moisture. The effect of internal restraint was taken into account in the thermal stress calculation. Internal restraints caused by the variation in moisture content and the

presence of reinforcing steel in the concrete were not considered.

The strain due to internal restraint at various locations in the barrier wall was calculated using Eq. [1] to [3] with the following modification to Eq. [2]: H was replaced by the half-thickness of the barrier wall, and d by the horizontal distance from the center of the cross section of the barrier wall. This modification reflected the fact that the degree of internal restraint is maximum ($K_R = 1$) at the center of the wall and decreases towards the faces.

Temperature

Internal heat due to cement hydration – The heat produced by cement hydration can generate large temperature gradients in concrete elements, resulting in significant stress due to internal restraint (Lachemi and Aïtcin 1997). The heat of hydration can also result in stress due to external restraint, since it produces a rise in temperature followed by a rapid cooling, resulting in temperature differences between the barrier wall and the deck slab. The effect of heat of hydration was evaluated using the adiabatic temperature-rise curves given in Fig. 2.3 of ACI 207 (1995), which express the increase in temperature over time of concretes cured under adiabatic condition. As the curves are given for a concrete containing only 223 kg/m^3 of cement, the selected curve was adjusted for a cement content of 450 kg/m^3 assuming that the total quantity of heat generated at any age is directly proportional to the quantity of cement in the concrete mix.

Heat transfer by convection and radiation – Heat from various sources is exchanged between the concrete and its surroundings. Heat exchanges by convection and radiation were determined using Newton's law of cooling and the Stefan-Boltzmann law (CEB 1985), respectively. The following radiation components were taken into account: (i) concrete surface radiation, (ii) global solar radiation, (iii) global radiation reflected by earth, (iv) earth surface radiation, and (v) atmospheric radiation. The estimate of solar radiation was made using a sinusoidal function of time between sunrise and sunset (CEB 1985) which took into account the geographical location (45 degrees latitude), the time of the year (October), and the orientation of the exposed surfaces (front surface of the barrier wall facing west).

Determination of temperature profiles – The two-dimensional temperature profile in the cross section of the barrier wall as a function of time was calculated by solving the following differential equation:

$$[4] \qquad D_T\left(\frac{\partial^2 T}{\partial x^2}+\frac{\partial^2 T}{\partial y^2}\right)+q=\frac{\partial T}{\partial t}$$

where D_T is the thermal diffusivity of concrete, q is the heat flux, T is temperature, t is time, and x and y are the distances through the thickness and height of the wall, respectively.

The numerical solution of Eq. [4] was obtained with a two-dimensional model of the wall cross section, divided in rectangular segments (six columns and eight rows), using the finite difference method with the following central operator:

$$[5] \qquad T_{i,j,\Delta t}=T_{i,j}+\frac{0.25}{k^2+1}\left[\begin{matrix}T_{i-1,j}-2T_{i,j}+T_{i+1,j}+\\ k^2\left(T_{i,j-1}-2T_{i,j}+T_{i,j+1}\right)\end{matrix}\right]$$

and

$$[6] \qquad \Delta t=\frac{\Delta x^2}{4D_T\,(k^2+1)}$$

where $T_{i,,j,\Delta t}$ is the temperature of a segment located at the *i*th column and the *j*th row for a given time increment Δt; Δx *and* Δy are the width and height of the segments in the horizontal and vertical directions, respectively, and k is the ratio $\Delta x/\Delta y$.

This central operator, which is typically used to solve thermal problems involving pure conduction heat transfer (q = 0), was selected for simplicity. A correction on the ambient air temperature, however, had to be applied before its use. The corrected air temperature was determined from the requirement that the convection heat transfer must equal the total heat transfer out of the volume considered, as shown in the following equation (CEB 1985):

$$[7] \quad h\,A(T_S - T_A^*) = h\,A(T_S - T_A) - \sum_i q_{r,i}$$

where h is the heat transfer coefficient, A is the surface area, T_S is the surface temperature, T_A is the ambient temperature, T_A^* is the corrected ambient temperature, and $q_{r,i}$ represents each individual part of the radiation heat flux. Solving for T_A^*, the corrected ambient temperature can be determined as follows:

$$[8] \quad T_A^* = T_A + \frac{\sum_i q_{r,i}}{h\,A}$$

Figure 7 illustrates the estimated temperature variations in the barrier wall at midheight for the 3 days following concreting. The combined effect of the formwork and heat of hydration during the first day was observed to cause a large temperature difference of 18°C between the front wall surface and the center, approximately 2 h before form removal.

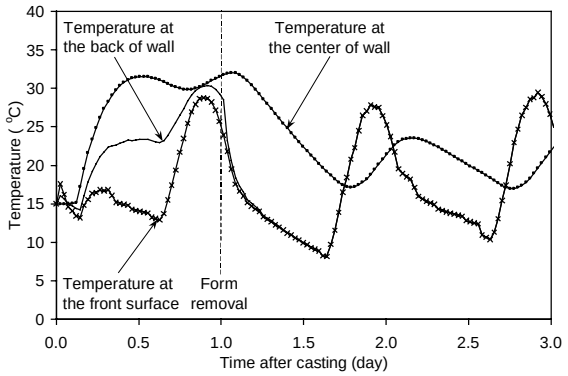

Fig. 7 – Estimated temperature variations in barrier wall at midheight

After that, the temperature differences decreased significantly, especially between the wall surfaces. The difference in temperature between wall surfaces is explained by the different thermal properties of the steel forms used at the front surface of the wall and the wood forms at the back. As illustrated in Fig. 7, for the first day, the steel forms at the front surface dissipated heat much more rapidly than the wood forms at the back. A direct consequence is the formation of adverse thermal gradients in the wall section, especially when the concrete tensile strength is still extremely low. The use of wood forms on both wall surfaces, and a concrete generating less heat of hydration would have reduced the thermal gradients in the first day.

A second observation is the marked effect of the estimated solar radiation and the measured ambient temperature on concrete temperature after form removal, with highest temperatures at the wall surfaces in the afternoon (t = 2.0 and 3.0 days) and highest temperatures in the wall center at night. A direct consequence of this pattern is the formation of alternating thermal gradients in the wall cross section.

Determination of thermal strain – The distribution of thermal strain in the barrier wall and in the portion of the slab near the wall/slab interface was obtained using the

product of the calculated temperature at the given location and the thermal expansion coefficient of the concrete under consideration. Because early-age concrete has a higher thermal expansion coefficient than mature concrete, a coefficient of 12 x 10^{-6}/°C was used for the young concrete of the barrier wall (RILEM-42-CEA 1981), and a coefficient of 9 x 10^{-6}/°C for the mature concrete of the deck slab, indicated for concrete with dolostone aggregates (85% dolomite).

Figure 8 illustrates the thermal strains at the front surface, the center, and the rear surface of the barrier wall at midheight. The thermal strains estimated for the time period before t = 0.5 day did not result in thermal stresses since concrete was not set. It is observed, however, that the significant temperature gradients that occurred after the concrete set translated into similar patterns of thermal strain gradients, that is, large contraction of the wall center restrained by expansion of the wall surfaces in the afternoon, and vice-versa at night.

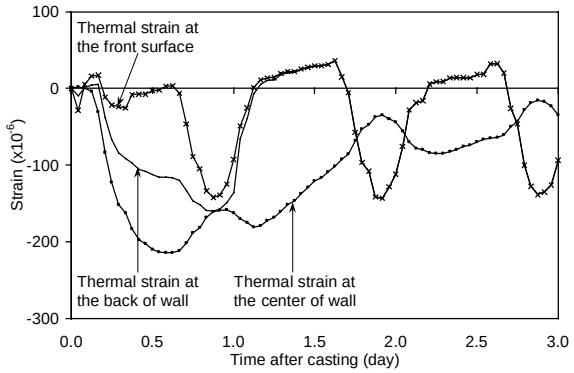

Fig. 8 – Estimated thermal strains in barrier wall at midheight

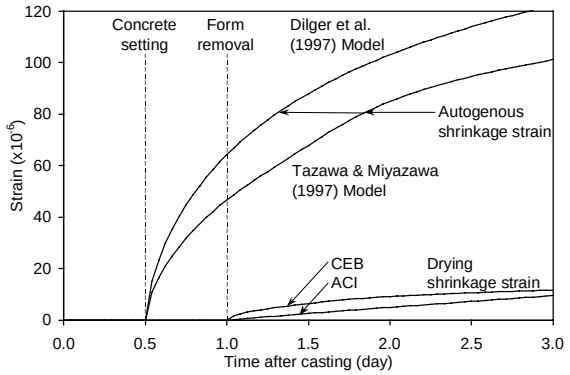

Fig. 9 – Estimated shrinkage strains in barrier wall

Shrinkage

Plastic shrinkage – Plastic shrinkage occurs before the final set of concrete if the concrete is not properly cured, and is restricted to the top layer of the barrier wall. Because concrete has a negligible elastic modulus before final setting, plastic shrinkage does not impose a significant stress and was therefore disregarded in this analysis.

Autogenous shrinkage – Autogenous shrinkage, caused by the uniform reduction in pore water content during the cement hydration, is significant for concrete of *w/c* less than 0.4 (Tazawa and Miyazawa 1993). The empirical models proposed by Tazawa and Miyazawa (1997) and by Dilger, Niitani, and Wang (1997) were used to estimate the autogenous shrinkage of the concrete in this study.

These models, applicable to concrete made with *w/c* lower than 0.5, take into account the effects of the *w/c*, the type of cement, and maturity (Tazawa and Miyazawa model only).

Figure 9 presents curves of the autogenous shrinkage strain calculated with both models from setting time at 0.5 day. Estimated values, ranged from 68 to 88 με at 1.5 days and from 101 to 122 με at 3 days, which are comparable to the tensile strain capacity of the concrete at these given times.

Drying shrinkage – Drying shrinkage, which is caused by the nonuniform drying of concrete after the end of curing and the removal of forms, increases with greater *w/c* (Le Roy, De Larrard and Pons 1996). Drying shrinkage was calculated using the empirical equations from both the CEB (1993a) and ACI 209R (1997) codes. Although these

equations were given for the estimation of total shrinkage, they were taken as estimates of only drying shrinkage in this analysis. The first reason is that the shrinkage strain, calculated at any given time with the ACI or CEB equations, was found to be much smaller than the corresponding autogenous shrinkage strain calculated under the same conditions with the Tazawa & Miyazawa (1997) model or the Dilger, Niitani, and Wang (1997) model. The second reason is that these ACI and CEB equations were developed from experimental data on normal strength concrete and cured under moist conditions for at least 7 days, by which time a large part of autogenous shrinkage had already taken place.

Figure 9 shows the strain due to drying shrinkage calculated for the conditions measured in the field using the CEB (1993a) and ACI (1997) models. Drying shrinkage was found to be negligible because of the short drying period considered (2 days), the concrete was of good initial quality and the thickness of the barrier wall was relatively large.

Traffic vibration

Two different sources of traffic vibration at the Vachon Bridge may have generated stress in the concrete of the barrier wall during construction: (i) the passage of heavy construction vehicles in the two lanes adjacent to the barrier wall; and (ii) regular traffic in the remaining lanes that were left open during bridge rehabilitation.

The dynamic strains caused by regular traffic were measured after bridge rehabilitation using strain gages embedded horizontally in the concrete of the barrier wall. Analysis of the longitudinal strains measured at several locations in the barrier wall indicated that maximum values occurred at the top of the barrier wall, at midspan, and during off-peak traffic hours (due to higher vehicle speeds).

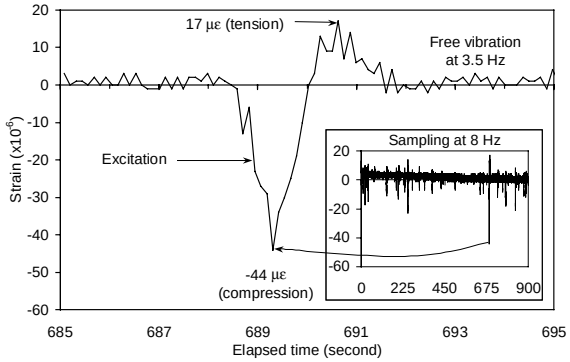

Fig. 10 – Estimated traffic-induced strain at top of barrier wall at midspan

Figure 10 illustrates the longitudinal strain monitored over a period of 900 s, with a gage located 100 mm from the top of the barrier wall at midspan. The largest strain excursion observed during this period is highlighted in the figure. Some stimulus, most likely the result of the rapid passage of a heavy truck, produced a deflection that resulted in a compressive strain of 44 με at the top of the barrier wall, followed by a dampened upward rebound that resulted in a tensile strain of 17 με. A calculation based on the development curve of the modulus of elasticity of concrete (Fig. 4) indicates that such a strain may have generated a stress exceeding the concrete tensile strength (Fig. 3) during the 3 h period following concrete setting, when the concrete was still extremely weak. Considering that the dynamic strains measured did not include that part of strain induced by heavy construction vehicles, and the fact that dynamic stresses are not reduced by concrete relaxation, the adverse effect of traffic vibration on the day following concreting should be given more attention in rehabilitation projects.

Relaxation

Relaxation of concrete in tension can be beneficial in some cases because it may reduce tensile stress caused by internal and external restraints (Saucier *et al.* 1997). As it is permitted by the CEB (1993a) code, the

following equation, originally developed to predict the relaxation of concrete in compression (CEB 1993b), was used to compute relaxation in tension:

[9]
$$R(t,\tau) = E(\tau)\left[1 - \frac{\phi(t,\tau)}{E_{w28}/E_w(\tau) + \chi(\tau)\cdot\phi(t,\tau)}\right]$$

where $R(t,\tau)$ represents the stress produced at time t by a constant unit strain applied at time τ, $\phi(t,\tau)$ is the creep coefficient at time t for a strain applied at time τ (in this case, $\phi(t,\tau)$ varied from 0, when $t-\tau = 0$, to 8, when $t-\tau$ = 3 days), $E_w(\tau)$ is the concrete modulus of elasticity of the barrier wall at time τ, E_{w28} is the concrete modulus of elasticity of the barrier wall at 28 days, and $\chi(\tau) = 0.8$ is an approximation of the concrete aging coefficient that has been commonly used by designers (CEB 1993b). Some computed relaxation functions are shown in Fig. 4 for times τ = 0.75, 1.0, 1.5, 2.0, and 2.5 days. The relaxation functions, which are similar to functions of the effective elastic modulus in creep problems, show a maximum at the application time of the strain increment considered, and decrease gradually with time ($t-\tau$). For example, to estimate the component of stress at any given time due to a strain applied at t = 2 days, one can use the relaxation function that starts at t = 2 days (Fig. 4) where, for instance, $R(2,2)$ is 25.2 GPa, and 1 day later, $R(3,2)$ is 18.9 GPa.

STRUCTURAL MODELING OF TOTAL STRESS

The aforementioned effects were integrated into a global structural model used for the prediction of the total stress over time in the barrier wall concrete. Deflection of the deck slab due to the weight of the barrier wall was not considered, as it almost entirely occurred before setting of the new concrete, therefore inducing no stresses in the barrier wall.

The stress σ at time t caused by the strain ε_R applied at time τ was calculated as:

[10]
$$\sigma(t,\tau) = \int_{\tau}^{t} R(t,\tau)\, d\varepsilon_R(\tau)$$

The solution of Eq. [10] was obtained using an incremental algorithm with time increments of 0.024 day. The principle of stress superposition was used to permit the addition of individual stresses from various sources and to take into account the cumulative relaxation of the stress for each new strain increment. The total stress as a function of time was thus calculated using the following model:

[11]
$$\begin{bmatrix} R_{i,i} & R_{i,i+1} & \cdots & R_{i,n} \\ R_{i+1,i} & R_{i+1,i+1} & \cdots & R_{i+1,n} \\ \vdots & \vdots & \ddots & \vdots \\ R_{n,i} & R_{n,i+1} & \cdots & R_{n,n} \end{bmatrix}$$
$$\begin{bmatrix} \Delta\varepsilon_{thi,i} & \Delta\varepsilon_{the,i} & \Delta\varepsilon_{as,i} & \Delta\varepsilon_{ds,i} \\ \Delta\varepsilon_{thi,i+1} & \Delta\varepsilon_{the,i+1} & \Delta\varepsilon_{as,i+1} & \Delta\varepsilon_{ds,i+1} \\ \vdots & \vdots & \vdots & \vdots \\ \Delta\varepsilon_{thi,n} & \Delta\varepsilon_{the,n} & \Delta\varepsilon_{as,n} & \Delta\varepsilon_{ds,n} \end{bmatrix} \begin{Bmatrix} 1 \\ 1 \\ 1 \\ 1 \end{Bmatrix} +$$
$$\begin{Bmatrix} E_{w,i}\cdot\varepsilon_{tv,i} \\ E_{w,i+1}\cdot\varepsilon_{tv,i+1} \\ \vdots \\ E_{w,n}\cdot\varepsilon_{tv,n} \end{Bmatrix} = \begin{Bmatrix} \sigma_{T,i} \\ \sigma_{T,i+1} \\ \vdots \\ \sigma_{T,n} \end{Bmatrix}$$

where the subscript i represents a time increment from 1 to n, R is the value of the relaxation function (Eq. [9]), $\Delta\varepsilon_{thi}$ is the thermal strain increment due to internal restraint, $\Delta\varepsilon_{the}$ is the thermal strain increment due to external restraint, $\Delta\varepsilon_{as}$ is the autogenous shrinkage strain increment, $\Delta\varepsilon_{ds}$ is the drying shrinkage strain increment, ε_{tv}

is the maximum tensile strain due to traffic vibration, and σ_T is the total stress.

Consideration of cracking

To account for the effect of progressive cracking on the degree of tensile restraint, the value of L in Eq. [2] was replaced by the calculated value of the average crack spacing at any given time. For instance, before cracking, the length L was set to the distance between expansion joints (34 m) and subsequently divided by 2 each time the total stress in the middle cross section between two consecutive cracks exceeded the concrete tensile strength. The residual tensile stress in the middle cross section therefore became rapidly negligible after several new occurrences of cracks. Stress release due to progressive cracking, however, was assumed not to occur in compression since the cracks are closed.

Determination of total stress

Figure 11 illustrates the estimated total stress at the base, at midheight, and at the top of the front surface of the barrier wall during the 3 days following concreting. Due to progressive cracking, these curves represent the residual concrete stresses in a cross section located midway between 2 consecutive cracks near the midspan of the barrier wall. According to the analysis, full height cracking occurred shortly after concrete setting and also at t = 1.1 days. The last estimated occurrence of cracking is not too different from the time at which cracks were first observed in the field (1.5 days). A similar level of tensile stress was estimated in the barrier wall between t = 2.1 and 2.7 days; however, no additional cracking resulted due to the increase in tensile strength.

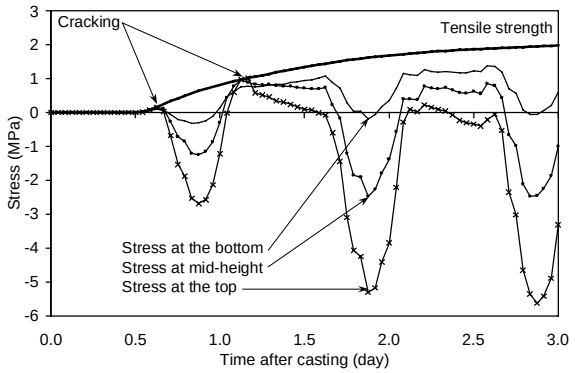

Fig. 11 – Estimated total stress at front surface of barrier wall near midspan

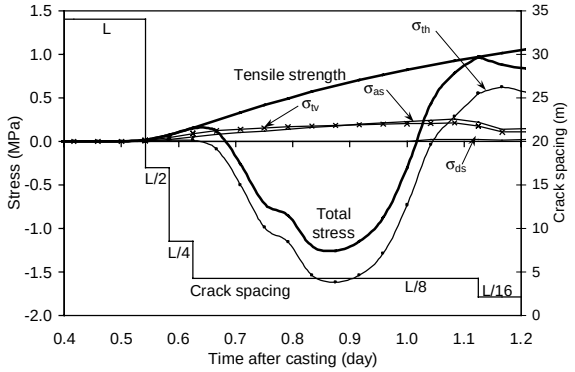

Fig. 12 – Estimated stress components in barrier wall (front surface, midheight, midspan)

Figure 12 presents a closer look at the stress at the same location in the barrier wall for a critical period of time, which shows separate components of stress, such as thermal stress σ_{th}, autogenous shrinkage stress σ_{as}, drying shrinkage stress σ_{ds}, and traffic vibration-induced stress σ_{tv}. An additional curve is superposed to illustrate the occurrence of progressive cracking.

According to the structural model, three series of cracking occurred in the first 3 h after setting of concrete. At this very early age, however, it is likely that the model may have underestimated the reduction of stress due to relaxation. On the other hand, stress due to traffic vibration, which is not reduced by relaxation of concrete, was most likely responsible for the cracking at this very early age.

A final series of cracking was estimated to occur at t = 1.1 days. At this time and location in the barrier wall, thermal stress was found to be the most important cause of cracking, followed by autogenous shrinkage stress and vibration-induced stress. Drying shrinkage stress was found negligible for the reasons stated previously. The model estimated a final crack spacing of 2 m (L/16). This compares with field observations where an average spacing of 0.8 m was measured along the wall.

DISCUSSION

As described, the concrete used for the reconstruction of the barrier walls had a cement content of 450 kg/m^3 and a *w/c* of 0.36, which is typical of field high-performance concrete. High concrete strengths are not necessary in bridge barrier walls since their function is not to support other parts of the bridge, but to assure safety in case of collision. A concrete with a lower amount of cement or higher *w/c* than the one used in the Vachon Bridge barrier walls would have produced less thermal and autogenous shrinkage stresses and, ultimately, less severe cracking.

On the other hand, the potential increase in durability of high-performance concrete may be of significant interest in reinforced concrete bridges, especially in areas where deicing salt are used. This analysis, however, confirms that the use of high-performance concrete does not in itself assure the durability of the barrier walls. The potential for improvements in concrete durability can be achieved only if appropriate construction techniques are used. Early-age transverse cracking due to excessive thermal stresses or restrained shrinkage may overshadow the expected superior durability of the concrete used.

CONCLUSIONS

The use of analytical models, supported by field data, led to a better understanding of the problem of early-age cracking observed at the Vachon Bridge. The main conclusions are:

- Thermal stress, due to steep temperature gradients through the barrier wall, was identified as the main factor responsible for the early-age cracking. Possible reasons are the use of a concrete with a high cement content, the use of formwork having different thermal properties (wood panels on one side and steel panels on the other), and the early removal of the formwork after 1 day, which accentuated the detrimental cooling of the barrier wall after hydration peak.
- Autogenous shrinkage seems to have contributed significantly to cracking. A concrete with a *w/c* somewhat higher than the one used would have been preferable for the construction of the barrier walls.
- Dynamic deck deflections and resulting strains due to traffic vibration may have contributed to cracking at midspan, especially during the few hours following concrete setting, when concrete was still very vulnerable to cracking. Experimental research is required to confirm this statement.
- Drying shrinkage was found to be negligible in the barrier wall. This was due to the short period of drying considered (2 days), the good initial quality of the concrete, and the relatively large wall thickness.
- This study confirms that the use of high-strength concrete does not in itself assure the durability of bridge barrier walls. Use of appropriate construction techniques is essential to improve concrete durability.

ACKNOWLEDGEMENTS

The authors wish to acknowledge the contribution of *Ministère des transports du Québec*, the bridge owner. The technical support provided by Ted Hoogeveen and Rock Glazer of NRC/IRC is greatly appreciated.

REFERENCES

ACI Committee 207 (1995): « Effect of restraint, volume change and reinforcement on cracking of mass concrete (207.2R-95), » ACI, Farmington Hills, Mich., 26 p.

ACI Committee 209 (1997): «Prediction of creep, shrinkage, and temperature effects in concrete structures (209R-92) (Reapproved 1997),» ACI, Farmington Hills, Mich., 47 p.

Carlson, R.W., and Reading, T.J. (1988): « Model Study of Shrinkage Cracking in Concrete Building Walls, » ACI Structural Journal, V. 85, No. 4, July-August, pp. 395-404.

CEB (1985): « Thermal effects in concrete structures, » *Information Bulletin No. 167*. Euro-International Concrete Committee, Lausanne, 122 p.

CEB (1993a): « CEB-FIP Model Code 1990, » *Information Bulletin No. 213/214*, Euro-International Concrete Committee, Lausanne, 437 p.

CEB (1993b): « Structural Effects of Time-Dependent Behaviour of Concrete, » *Information Bulletin No. 215*, Euro-International Concrete Committee, Lausanne, 297 p.

Cusson, D. and Mailvaganam, N. (1999): « Monitoring Techniques for Evaluation of Corrosion Inhibiting Systems in Reconstructed Concrete Bridge Barrier Walls, » *Concrete International*, V. 21, No. 8, August, pp. 41-47.

Dilger, W.H., Niitani, K. and Wang, C. (1997): « Creep and shrinkage model for high-performance concrete, » *International Conference on Engineering Materials*, Ottawa, pp. 615-630.

Lachemi, M. and Aïtcin, P.-C. (1997): « Influence of ambient and fresh concrete temperature on the maximum temperature and thermal gradient in a high-performance concrete structure, » *ACI Materials Journal*, V. 94, No. 2, March-April, pp. 102-110.

Le Roy, R., De Larrard, F. and Pons, G. (1996): « The AFREM Code Type Model for Creep and Shrinkage of High-Performance Concrete, » *4th International symposium on Utilization of High-Strength/High-Performance Concrete*, Paris, pp. 387-396.

RILEM 42-CEA (1981): « Properties of set concrete at early-ages – State of the Art Report, » *Matériaux et Constructions*, V. 14, No. 84, pp. 399-450.

Saucier, F., Claireaux, F., Cusson, D. and Pigeon, M. (1997): « The challenge of numerical modeling of strains and stresses in concrete repairs, » *Cement and Concrete Research*, V. 27, No. 8, pp. 1261-1270.

Tazawa, E. and Miyazawa, S. (1993): « Autogenous shrinkage of concrete and its importance in concrete technology, » *Creep and Shrinkage of Concrete*, Z.P. Bazant and I. Carol, eds., London, pp. 159-168.

Tazawa, E. and Miyazawa, S. (1997): « Influence of curing conditions on autogenous shrinkage of concrete, » *International Conference on Engineering Materials*, Ottawa, V. 1, pp. 373-384.

TRB (1996): « Transverse cracking in newly constructed bridge decks, » *National Co-operative Highway Research Program Report 380*, Transportation Research Board, National Academy Press, Washington, 126 p.

NOTATIONS

A	surface area
A_s	effective cross-sectional area of deck slab
A_w	cross-sectional area of barrier wall
a	coefficient depending on *w/c*
b	coefficient depending on *w/c*
c	coefficient depending on cement type
D_T	thermal diffusivity of concrete
d	vertical distance from bottom of wall
E_s	elastic modulus of concrete in the slab
E_w	elastic modulus of concrete in wall
E_{w28}	elastic modulus of concrete in wall at 28d
f_c	mean compressive strength of concrete
f_t	mean tensile strength of concrete
G_{DT}	daily-total global radiation
H	height of barrier wall
h	heat transfer coefficient
K_R	degree of restraint
k	ratio $\Delta x/\Delta y$
L	length of barrier wall
L	spacing between two adjacent cracks
q	heat flux
q_c	heat flux due to convection
q_r	total heat flux due to radiation
q_{ra}	heat flux due to atmospheric radiation
q_{rc}	heat flux due to concrete surface radiation
q_{re}	heat flux due to earth surface radiation
q_{rr}	heat flux due to radiation reflected by earth
q_{rs}	heat flux due to global solar radiation
R	relaxation of concrete
R_s	stiffness ratio
T	temperature
T_A	ambient temperature
T_A*	corrected ambient temperature
T_S	surface temperature
t	time or age of concrete after casting
t_d	time at start of concrete drying
t_o	time of concrete setting
t_{red}	reduced hours of sunlight during day
t_T	maturity of concrete
w/c	water-cementitious materials ratio
x	distance across wall thickness
y	distance across wall height
β_c	creep development coefficient
β_{cc}	strength development coefficient
β_s	shrinkage development coefficient
χ	aging coefficient
$\Delta\varepsilon_{as}$	increment of autogenous shrinkage strain
$\Delta\varepsilon_{ds}$	increment of drying shrinkage strain
$\Delta\varepsilon_{the}$	increment of thermal strain due to ext. restraint
$\Delta\varepsilon_{thi}$	increment of thermal strain due to int. restraint
Δt	time increment
Δx	segment width
Δy	segment height
ε_{as}	autogenous shrinkage strain
ε_{ds}	drying shrinkage strain
ε_{dso}	notional drying shrinkage strain
ε_f	free strain
ε_R	restrained strain
ε_{tv}	max. tensile strain due to traffic vibration
ϕ	creep coefficient
ϕ_o	notional creep coefficient
γ	coefficient depending on cement and admixture
ρ_g	ratio of reinforcement in the cross section
σ	stress
σ_{SB}	Stefan-Boltzmann radiation constant
σ_T	total stress
τ	time of strain application

APPENDIX 1 – LIST OF SUPPLEMENTARY EQUATIONS USED IN ANALYSIS

Thermal analysis (heat flux)

Convection: $q_c = h\,A(T_S - T_A)$

Concrete surface radiation: $q_{rc} = 0.88\,\sigma_{SB}\,A T_S^4$

Global solar radiation: $q_{rs} = 0.65 \cdot A\left[G_{DT}\,\frac{\pi}{2\,t_{red}}\sin\left(\frac{180\,t}{t_{red}}\right)\right]$

Global radiation reflected by earth: $q_{rr} = 0.88 \cdot 0.25\,A\left[G_{DT}\,\frac{\pi}{2\,t_{red}}\sin\left(\frac{180\,t}{t_{red}}\right)\right]$

Earth surface radiation: $q_{re} = 0.88 \cdot 0.99\,\sigma_{SB}\,A T_A^4$

Atmospheric radiation: $q_{ra} = 0.88 \cdot 0.94\,\sigma_{SB}\,A T_A^4$

Stress analysis

Concrete maturity:
($T_{\Delta ti}$ in °C) $t_T = \sum_{i=1}^{n} \Delta t_i \exp\left[\frac{-4000}{273 + T_{\Delta t_i}} + 13.65\right]$

Strength development coefficient:
(t_T in days) $\beta_{cc}(t) = \exp\left(c - c\sqrt{\frac{28}{t_T}}\right)$

Tensile strength development:
(f_c in MPa) $f_t(t) = \beta_{cc}(t) \cdot 1.4\left(\frac{f_c}{10}\right)^{2/3}$

Elastic modulus development:
(f_c in MPa) $E_w(t) = \sqrt{\beta_{cc}(t)} \cdot 21500\left(\frac{f_c}{10}\right)^{1/3}$

Drying shrinkage: $\varepsilon_{ds}(t, t_d) = \varepsilon_{dso}\,\beta_s(t_T - t_d)$ & Eqs. 2.1-75–2.1-79 in CEB (1993a)

Creep coefficient: $\phi(t, \tau) = \phi_o\,\beta_c(t_T - \tau)$ & Eqs. 2.1-65–2.1-72 in CEB (1993a)

Autogenous shrinkage:

Dilger et al. (1997) model:
($0.15 \le w/c \le 0.40$)
(t_T in days) $\varepsilon_{as}(t) = 700\exp\left(-3.5\frac{w}{c}\right)\frac{t_T^{0.7}}{16.7\left(-0.04 - \frac{w}{3c}\right) + \left(1.04 - \frac{w}{3c}\right)t_T^{0.7}}$

Tazawa et al. (1997) model:
($0.20 \le w/c \le 0.50$)
(t_T and t_o in days) $\varepsilon_{as}(t) = \gamma\,\frac{3070}{10^6}\exp\left[-7.2\left(\frac{w}{c}\right)\right] \cdot \left[1 - \exp\left(-a\,(t_T - t_o)^b\right)\right]$

APPENDIX 2 – LIST OF PARAMETERS USED IN ANALYSIS

Heat transfer analysis

Conduction heat transfer

Initial temperature of concrete:	15 °C
Thermal diffusivity of concrete:	0.0478 m^2/day
Width of the segments:	0.080 m
Height of the segments:	0.129 m

Convection heat transfer

Wind speed:	3 m/s
Transfer coefficient of ambient air:	17.60 W/m^2/°C
Transfer coefficient of the steel form:	17.57 W/m^2/°C
Transfer coefficient of the wood form:	5.26 W/m^2/°C
Thickness of the steel form:	5 mm
Thickness of the wood form:	20 mm

Radiation heat transfer

Stefan-Boltzmann constant	5.67 x 10^{-8} W/m^2/°K^4
Long-wave emissivity of concrete	0.88
Short-wave emissivity of concrete	0.65
Emissivity of the atmosphere (with clouds)	0.94
Emissivity of the earth surface	0.99
Daily total of global radiation	8000 Wh/m^2
Reduced hours of sunlight (October, 45° latitude)	10.5 h

Stress analysis

28-day compressive strength of new concrete (measured):	45 MPa
Elastic modulus of old concrete (assumed):	35 GPa
Thermal expansion coefficient of new concrete (1 to 7 days of age):	12x10^{-6}/°C
Thermal expansion coefficient of old concrete (dolostone aggregate):	9x10^{-6}/°C